Oxyfluoride glasses obtained through incorporation of CaF2CaF_2 into photovoltaic cover glass melts

Rafaela Valcarenghi, Brenno Silva Greatti, Robson Ferrari Muniz, Vitor Santaella Zanuto, Anna Paulla Simon, Ricardo Schneider, Raquel Dosciatti Bini, Márcio Antônio Fiori, Maxence Vigier, Emmanuel Véron, et al.

Received: 19 May 2025 | Revised: 5 August 2025 | Accepted: 27 August 2025

DOI: 10.1111/jace.70252

Journal of the American Ceramic Society

RESEARCH ARTICLE

Oxyfluoride glasses obtained through incorporation of CaF_2 into photovoltaic cover glass melts

Rafaela Valcarenghi[1] | **Brenno Silva Greatti**[2] | **Robson Ferrari Muniz**[2] | **Vitor Santaella Zanuto**[2] | **Anna Paulla Simon**[1,3] | **Ricardo Schneider**[4] | **Raquel Dosciatti Bini**[1] | **Márcio Antônio Fiori**[1,5] | **Maxence Vigier**[6] | **Emmanuel Veron**[6] | **Mathieu Allix**[6] | **Marcelo Sandrini**[1] | **Marcos Paulo Belançon**[1]

[1]Universidade Tecnológica Federal do Paraná, Paraná, Brazil

[2]Universidade Estadual de Maringá, Maringá, Paraná, Brazil

[3]Instituto Federal do Paraná, Barracão, Brazil

[4]Universidade Tecnológica Federal do Paraná, Toledo, Brazil

[5]Universidade da Região de Chapecó, Chapecó, Brazil

[6]Laboratoire CEMHTI, Orléans, France

Correspondence
Marcos Paulo Belançon, Universidade Tecnológica Federal do Paraná, Pato Branco, 85503-390, Paraná, Brazil.
Email: marcosbelancon@utfpr.edu.br

Funding information
Coordenação de Aperfeiçoamento de Pessoal de Nível Superior; Conselho Nacional de Desenvolvimento Científico e Tecnológico, Grant/Award Numbers: 304060/2023-2, 402473/2023-0, 409475/2021-1

Abstract

The glass industry has limited options to mitigate its environmental footprint, and the demand for cover glass to produce photovoltaic panels continues to increase. Currently, the majority of this special type of glass is not being recycled; therefore, this work proposes to reuse it as raw material to obtain oxyfluoride glasses. The incorporation of CaF_2 and the increasing Na_2CO_3 content resulted in a melting temperature of about 1200°C, significantly lower than in soda-lime glasses, contributing to the environmental benefits of reusing end-of-life cover glass. The obtained samples show high transparency and thermal stability, allowing the cover glass to make up to 80% of its weight. XRF analysis was employed to determine the elemental composition of the samples, while XRD and Raman indicated that by adding CaF_2 the glass network was depolymerized. In situ XRD as a function of temperature showed the formation of a few crystalline phases in these oxyfluoride samples, evidencing their potential to be explored as a matrix to obtain different glass-ceramics. The combination of the glass properties indicates that this method and the resulting material can contribute to reducing the environmental impact of the glass industry. Furthermore, new glass or glass-ceramic materials can be obtained at a reduced temperature compared to soda-lime glass, while cover glass, being the primary raw material, could reduce the need to extract minerals from nature.

KEYWORDS

glass recycling, glass waste management, glass-ceramics, silicate, waste reduction

1 | INTRODUCTION

The world consumes over 130 million tons of glass annually, or about 16 kg per capita. Container and flat glass account for about 80% of global glass production and are estimated to release more than 60 million tons of carbon dioxide into the atmosphere, primarily due to intensive heating of raw materials.[1,2] Soda-lime is the most common glass, and the industry has limited options to mitigate its environmental footprint. To produce 1 kg of soda-lime glass, the carbonates present in the raw materials will emit around 0.15 kg of CO_2, while the huge amount of energy required to heat and melt (~ 1500°C) the glass results in another 0.45 kg, primarily due to the combustion of fossil fuels.[1,3] Although clean electricity and hydrogen can be employed, these alternatives have yet to be demonstrated on an industrial scale.[2,4]

Though glass can be recycled indefinitely, doing so is often not feasible or attractive due to technical and economic reasons.[5,6] As discussed in our previous work,[7] highly transparent soda-lime is used as cover glasses (CG) in solar energy applications, and these high-quality materials are facing the risk of being dumped in landfills once their demand continues to rise, while the options to reuse them are pretty limited. Additionally, glass production requires vast amounts of raw materials and mining is one of the most energy-intensive industries,[8] resulting in a severe environmental impact. These factors highlight the importance of recycling and reusing CG, turning end-of-life products into raw materials to keep them on the market, in a context of circular economy.[9–11]

Glasses other than soda-lime have been proposed as alternatives for solar energy applications, which could include new features such as spectral conversion to enhance silicon solar panel technology.[7] However, among dozens of proposed glass systems, silicates are the only ones based on abundant, affordable, and nontoxic minerals. The resulting glasses often exhibit high transparency and adequate chemical and mechanical resistance for solar energy applications. Reviewing the literature recently,[7,12] we concluded that modified soda-lime silicates are the most promising system that could meet the requirements needed for mass-scale industrial production, while providing new or enhanced properties that could reduce industry energy consumption, expand solar power production, and contribute significantly to sustainability goals.

An interesting silicate system, which we have already investigated, is achieved when CaF_2 is added to silica melts.[13,14] While modifiers such as CaO and Na_2O are well-known for reducing the melting temperature of silicates, the F provided by CaF_2 often replaces O, affecting the silica network.[15] Several studies have shown that CaF_2 incorporation reduces the melting temperature and viscosity of silicates,[15] while it can improve the microstructure[16] and promote or inhibit the formation of crystalline phases,[17,18] including nanocrystals.[19]

To address all the questions mentioned above, this work proposes using CGs from end-of-life solar panels as raw materials to produce oxyfluoride sodium calcium silicate glasses, achieved by incorporating CaF_2. Our methodology is simple; the obtained samples have high optical quality and allow a recycled fraction of raw materials as high as 80% of the final weight of the glass samples. Using CG as a raw material may contribute to the sustainability of the glass industry and positively impact the environment by reducing energy demand and the extraction of new raw materials from nature, ultimately reducing overall emissions and environmental footprint. Additionally, as we will show, these CG-derived materials may provide a platform for research and development of new glasses and glass-ceramics for several applications.

TABLE 1 Mass of each sample prepared in this work.

Sample	Cover-glass (g)	CaF_2 (g)	Na_2CO_3 (g)	Total (g)
CgCAF05	13.00	1.00	1.94	15.94
CgCAF12	12.25	2.45	1.83	16.53
CgCAF15	11.80	3.00	1.76	16.56
CgCAF18	11.30	3.50	1.69	16.49
CgCAF20	10.90	4.00	1.63	16.53

2 | MATERIALS AND METHODS

The weight of the compounds mixed to produce each sample is shown in Table 1, where the sample names refer to the mol% of CaF_2. The CG, sourced from photovoltaic panels previously studied,[20] was fragmented into particles approximately 5–10 mm in length. The reagents added to the mix were CaF_2 and Na_2CO_3, both from Sigma-Aldrich with 99.0% purity. To keep the ratio SiO_2/Na_2O approximately constant through all the samples, the Na_2CO_3 concentration was adjusted accordingly.

Reagents were mixed with CG in a platinum crucible and heated in a furnace, using a 10°C/min heating rate, with holding steps of 40 min at 200°C, 60 min at 500°C, 90 min at 800°C, and 120 min at 1200°C. This thermal profile was chosen to ensure a homogeneous fusion of the mixture and to avoid foaming or spillage during melting. After this stage, the molten glass was poured into a stainless steel mold and rapidly transferred to a second furnace maintained at 480°C, where it was kept for approximately 12 h

FIGURE 1 Samples investigated in this work, as prepared for analyses. The diameter of the discs is about 1.0 cm.

to relieve internal stresses. Upon cooling to room temperature, the samples were removed from the mold. Figure 1 shows a photograph of the obtained samples, which were cut, polished, or milled for the analyses.

The analytical techniques employed in this study encompass compositional, thermal, structural, and optical analyses. X-ray fluorescence (XRF) was used to determine the chemical composition of the samples. The analysis was performed on fused beads at approximately 1200°C (Panalytical, Axios). The beads were prepared from powdered material, previously ground to pass through a 325-mesh sieve, using lithium tetraborate as the flux. Additionally, loss-on-ignition analysis was carried out to account for volatile content up to 1000°C. DTA was performed in the temperature range of 50–900°C, using a heating rate of 10°C/min under a synthetic air atmosphere with a flow rate of 50 mL/min (TA Instruments, SDT Q600). The density of the samples was obtained using Archimedes' principle with distilled water at room temperature. Mass measurements were performed with an analytical balance with a precision of ± 0.1 mg (Kern ABT, 120-5DM).

Structural characterization was performed by X-ray powder diffraction (XRPD) on powdered samples. The analysis used CuKα radiation (λ= 1.5418 Å) at 40 kV and 15 mA, with a scanning rate of 5°/min, a step size of 0.02°, and a 2θ range of 5–80° (Rigaku. Miniflex 600). Also, in situ XRPD analysis was performed on powdered material to evaluate the temperature-dependent structural evolution. The measurements were conducted under air in the Bragg–Brentano θ–θ geometry, using Ni-filtered CuKα_1 radiation (λ = 1.5418Å), over a 2θ range of 15–60°, with a step size of 0.016° and a counting time of 0.5 seconds/step. A temperature step of 25°C was applied from 500 to 950°C. Data were collected on a Bruker-AXS D8 Advance diffractometer (Karlsruhe, Germany) equipped with an Anton Paar oven chamber (model HTK 1200N, Graz, Austria), which allows measurements up to 1473 K. The powdered samples were placed in a platinum-lined corundum sample holder, and the diffracted intensities were recorded using a LynxEye detector.

Optical characterization involved Raman spectroscopy, UV–Vis–NIR, and spectroscopic ellipsometry analysis. Raman spectra were collected on a Bruker–Senterra Raman microscope using a 532-nm laser at 20 mW, in the spectral range of 50–1542 cm^{-1}. A 20× objective lens was used for laser focusing, and the signal was integrated for 2 s. UV–Vis–NIR transmittance was measured in the spectral range of 190–3600 nm (Shimadzu, UV-3600i Plus), and the refractive index of the samples was determined by spectroscopic ellipsometry at an incidence angle of 55° (HORIBA, UVISEL Plus).

3 | RESULTS AND DISCUSSION

Although the CG is expected to be low-iron soda-lime glass, and the reagents added are quite pure, the samples were submitted to XRF analysis to confirm their composition. These results are shown in Table 2.

Assuming the CG composition obtained from the XRF analysis and the weights shown in Table 1, we can calculate the stoichiometric relations for CgCAF samples, which are very similar to those obtained experimentally by XRF. In this way, though fluorine is well known to be volatile, these results corroborate the assumption that no significant mass was lost during the melting process. As previously stated, we also aimed to keep the ratio SiO_2/Na_2O constant, and the XRF analysis confirms this; it lies in the range of ~3.5 to 3.7 for the samples.

Figure 2 presents the XRPD patterns for all glass samples. The absence of sharp peaks in all patterns confirms the amorphous nature of the samples, consistent with a glassy structural framework. These results are in agreement with previously reported diffractograms for glasses and glass-ceramics of similar compositions.[13,21,22]

Notably, the diffraction halos exhibit two overlapping broad bands, which can be more clearly distinguished by fitting the patterns with two Lorentzian curves, as shown in Figure 2, represented by the filled green and blue curves corresponding to bands centered at approximately 22° and 30°, respectively. The area ratio between the green and blue bands decreases from 1.16 for the CG sample to 0.69 for the CgCAF20 sample. In the CG sample, the most intense band is centered around 22°, whereas in samples with increasing CaF_2 content the band at 30° becomes more prominent. This behavior is likely associated with structural rearrangements driven by the incorporation of fluoride ions. As reported by Iwamoto and Makino,[23] fluoride ions in

TABLE 2 Composition obtained by XRF expressed as a percentage (mol%).

Compound	CG	CgCAF05	CgCAF12	CgCAF15	CgCAF18	CgCAF20
SiO_2	72.62	62.90	58.22	56.62	54.18	52.51
CaO	9.35	7.63	7.59	7.35	7.11	6.88
Na_2O	12.48	17.62	16.12	15.28	15.19	15.15
MgO	4.46	3.81	3.55	3.44	3.29	3.19
Al_2O_3	0.48	0.37	0.36	0.33	0.31	0.32
K_2O	0.32	0.26	0.26	0.22	0.24	0.24
CaF_2[a]	—	5.20	12.40	15.25	17.98	20.61

aThe CaF_2 concentration was estimated assuming that the Ca concentration obtained by XRF is the sum of CaO (from CG) plus CaF_2 (added).

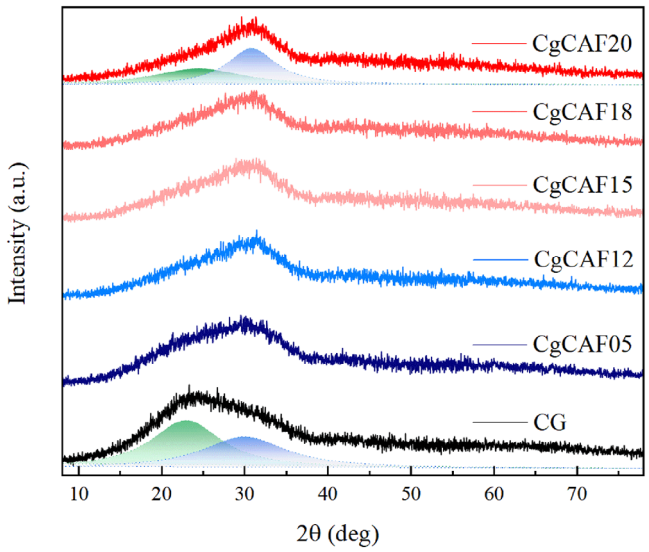

FIGURE 2 X-ray powder diffraction patterns.

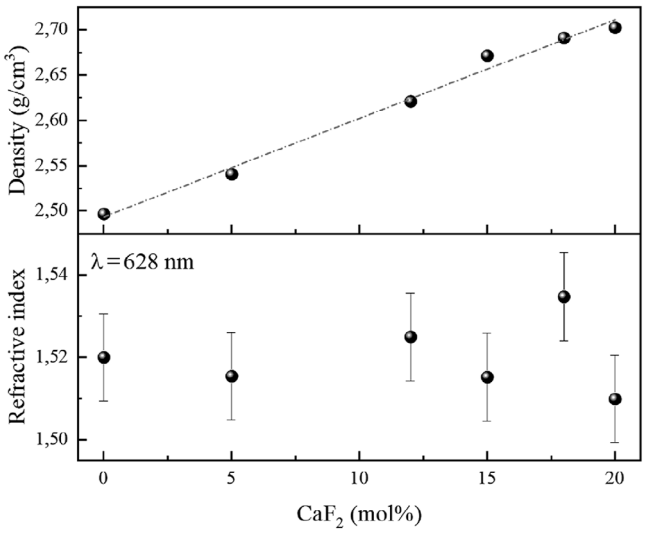

FIGURE 3 Mass density and refractive index at 628 nm of the samples as a function of the CaF_2 concentration. Error bars are negligible for the density in this range.

calcium fluorosilicate systems can engage in Si–F or Ca–F bonding. At lower CaF_2 concentrations, the formation of Si–F bonds is favored, whereas at higher concentrations, Ca–F interactions become more prominent. This transition is accompanied by a change in the fluoride coordination environment, from fourfold coordination, characteristic of a CaF_2-type quasi-lattice, to sixfold coordination typical of a NaCl-type quasi-lattice. Notably, the NaCl-type structure possesses smaller average lattice parameters than the CaF_2-type configuration. According to Bragg's law, a reduction in the lattice spacing results in a shift of diffraction features towards higher 2θ angles. Nonetheless, confirmation of this hypothesis requires more comprehensive structural analyses, including advanced modeling approaches.

As demonstrated in Table 2, CgCAF samples have a significantly lower proportion of SiO_2 compared to the CG as the CaF_2 concentration increases. Figure 3 presents the mass density and refractive index at 628 nm as a function of the CaF_2 concentration.

The mass density of the samples increases linearly with the addition of CaF_2, with an experimental uncertainty of ± 0.001 g/cm^3, which renders the associated error bars negligible in the graphical representation. The linear increase in density observed with increasing CaF_2 content in the multicomponent soda-lime glass matrix arises from the combined effects of compositional modifications and structural rearrangements. Specifically, the gradual replacement of the lighter network forming, SiO_2 by CaF_2, along with concurrent variations in the concentrations of other constituents such as Na_2O, CaO, and MgO, introduces heavier cations (e.g., Ca^{2+}, Na^+) and larger anions (F^-) into the glass structure. These changes lead to an increase in the average molar mass and promote a partial depolymerization of the silicate network, thereby enhancing atomic packing efficiency. The resulting structural compaction is corroborated by the shift of the amorphous halo to higher 2θ values in the XRPD patterns, indicating a reduction in the mean interatomic distances. At the same time, the refractive index remained constant ($n \sim$

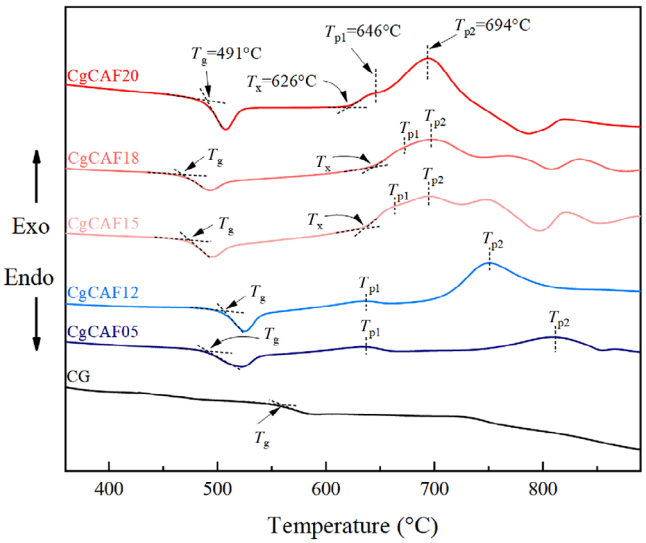

FIGURE 4 Differential thermal analysis of CG and CgCAF samples.

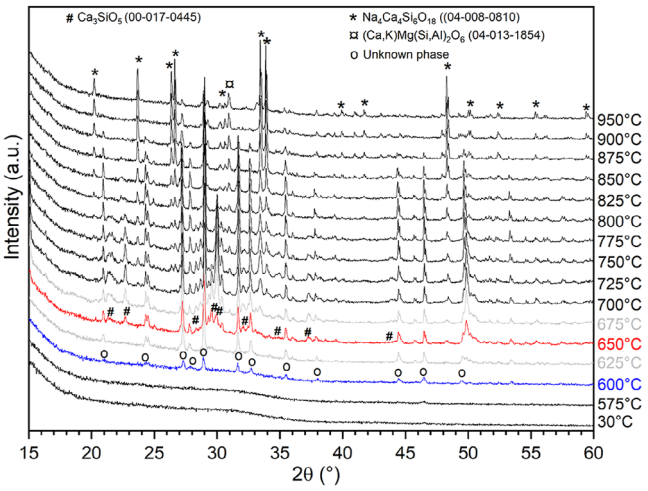

FIGURE 5 In situ XRPD performed on the CgCAF12 sample.

TABLE 3 Thermal parameters of glass samples.

Sample	T_g (°C)	T_x (°C)	$T_p(1)$ (°C)	$T_p(2)$ (°C)	T_x–T_g (°C)
CG	560	—	—	—	—
CgCAF05	491	—	636	812	—
CgCAF12	507	—	637	751	—
CgCAF15	475	636	664	695	161
CgCAF18	469	644	673	697	175
CgCAF20	491	626	646	694	135

1.52), within the error margins. Muniz et al.[13] have investigated sodium calcium silicate glasses containing amounts of CaF_2 similar to those in the present work, showing about the same mass density and a smaller refractive index (1.47).

Figure 4 presents the thermograms of all samples, including CG, where the key events T_g (glass transition), T_x (onset of crystallization), and T_p (crystallization peak) are also indicated. A summary of the characteristic temperatures identified for all samples is shown in Table 3. However, in these experiments, T_x could not be identified for the CG, CgCAF05, and CgCAF12 samples.

As can be seen, in all CgCAF samples, it is possible to identify two crystallization peaks, a result widely observed in the literature on silicates containing CaF_2,[13,16] as well as a significant reduction in the glass transition temperature (~50–90°C).

It is essential to note the satisfactory glass stability (T_x–T_g) observed in these samples, suggesting a suitable working temperature that may enable these materials to be produced in different shapes and sizes. Although T_x could not be identified.

An in situ high-temperature XRPD study was performed on the CgCAF12 sample to investigate its crystallization characteristics under thermal treatment. The corresponding diffraction patterns are shown in Figure 5.

Consistent with DTA measurements, a crystalline phase appears at 600°C. Nevertheless, we cannot identify this phase using the ICDD PDF5 database. Additional work will be necessary to elucidate this point. The proportion of this unknown phase increases until 800°C and after decreases but is present in small amounts at 950°C. At 650°C, we observe the crystallization of C3S (Ca_3SiO_5 JCPDS file 00-017-0445), which disappears at 800°C. The combeite phase ($Na_4Ca_4Si_6O_{18}$ JCPDS file 04-008-0810) crystallizes around 700°C, and its proportion increases until 950°C, finally becoming the main phase at high temperature. After this experiment, the PXRD diagram collected at room temperature shows the presence of combeite and a minimal amount of akermanite (JCPDS file 01-079-2425). Some of these phases have been linked to intriguing features, such as antimicrobial activity.[24] This indicates that CG-derived materials may also result in glass-ceramics with unique properties, which we will explore in future work.

Figure 6 shows the Raman spectra recorded for all samples, along with deconvolution using a multipeak Gaussian fit applied to the CgCAF05 sample (including the individual Gaussian components) as a representative example. Each Raman spectrum was fitted using 11 Gaussian components labeled (a–k) in the figure. This number was chosen based on the stability of the fitting process, as additional components did not significantly improve the quality of the fit. A weak band (g), located at approximately 870 cm^{-1}, could not be fitted for the CgCAF05 sample. The Raman scattering of the studied glasses is dominated by bands in the 550–750 cm^{-1} range (c, d, and

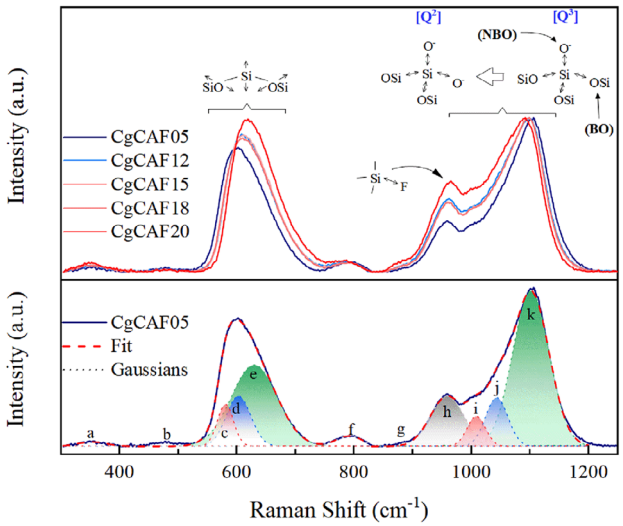

FIGURE 6 Raman spectra of CgCAF samples.

e) and in the 900–1200 cm^{-1} range (h, i, j, and k). Raman spectroscopy has proven to be a powerful technique for the structural investigation of silicate glasses,[25–27] although multiple overlapping bands pose a significant challenge for complete spectral interpretation.

The bands within the 900–1200 cm^{-1} range (h, i, j, and k) are attributed to symmetric stretching vibrations of Si'O bonds in various [SiO_4] tetrahedral units, commonly referred to as Q^n bands (where n = 0–4), with n denoting the number of bridging oxygens per tetrahedron.[27,28] It is well established that the band near 1100 cm^{-1}, associated with the Si–O vibration involving bridging oxygens, shifts to lower frequencies—or new bands emerge in lower frequency regions—due to the disruption of Si–O–Si linkages.[29] Furthermore, the primary determinant of Raman band frequency within this range is the force constant of the Si–NBO (nonbridging oxygen) bond. In silicate glasses containing CaF_2, the substitution of oxygen atoms by fluorine distorts the silicon's local electronic environment due to the higher electronegativity of fluorine. This distortion weakens the remaining Si–O bonds within the tetrahedra, leading to lower bond force constants and, consequently, lower associated vibrational frequencies.[30] This effect explains the slight "k" band shift with increasing CaF_2 concentration; this behavior was also observed by Muniz et al.[31] for a similar glass composition.

On the other hand, the Si–F bond behaves similarly to the Si–O bond, and the stretching vibration of the Si–F bond in SiO_3F^- tetrahedra typically appears near 950 cm^{-1} in fluorine-containing silica glasses.[30,32] Therefore, the formation of Si–F bonds may influence the frequencies of Si–O related vibrations and could account for the systematic increase in intensity observed for band "h" (~960 cm^{-1}) as CaF_2 content increases.

The bands in the 600 cm^{-1} region (c, d, and e) are assigned to symmetric vibrations of bridging oxygens in Si–O–Si linkages.[28,31] In conventional soda-lime glasses, bands near 500 and 560 cm^{-1} are attributed to bending motions of Si–O–Si in highly polymerized tetrahedral structures (Q^4 and Q^3 species), while bands above 600 cm^{-1} are typically associated with Si–O bending in depolymerized [SiO_4] tetrahedra (Q^2 species).[28,33] Although the Raman spectra of the intermediate samples (with CaF_2 contents ranging from 12.15 to 18 mol%) exhibit negligible variation among themselves, a notable shift of approximately 20 cm^{-1} is observed in the position of bands "e" and "k" when comparing the initial (CgCAF05) and final (CgCAF20) samples of the series. This spectral evolution indicates an increase in the fraction of NBO relative to total oxygens, suggesting a progressive depolymerization of the silica network with increasing CaF_2 content.[13,34,35] Such behavior implies significant structural modifications, including the possible formation of new Q^n species or phases, or a substantial reorganization within the silicate network.

The observed low-intensity Raman bands can also be identified. Band "a," located near 350 cm^{-1}, is attributed to the vibrations of the network-modifying cations.[31] Although weak, its integrated area increases linearly with the CaF_2 concentration. Band "f," observed at 800 cm^{-1} and invariant concerning CaF_2 content, is assigned to the Si–O stretching with dominant Si atom motion.[36] Symmetric stretching vibrations of Ca–F bonds are expected to appear around 485 cm^{-1} (band "b").[30] However, due to the highly ionic character of the Ca–F bond, Raman bands associated with these vibrations exhibit low intensity and barely to no variation is observed as a function of CaF_2 content in the glass compositions studied.

Finally, samples of about 0.6 mm were used to measure the light transmittance in the range 190–3500 nm. These spectra are shown in Figure 7, demonstrating the overall high transmittance of the CgCAF samples.

As shown in Figure 3, the refractive index of these samples is $n \cong 1.5$, which translates to reflection losses of about 4% at each air–glass interface. As can be seen, the transmittance remains near 90% from UV to NIR, evidencing the high optical quality of the CgCAF samples in this range. As transmittance (~90%) plus reflection (~8%) accounts for about 98% of the incoming light, it can be concluded that the absorption and scattering losses are pretty low in these samples. The inset in Figure 7 also highlights the wider transmittance window in the UV range of CgCAF samples compared to the original soda-lime glass, which may be associated with changes in the glass structure and could point to potential applications in UV-related technologies.

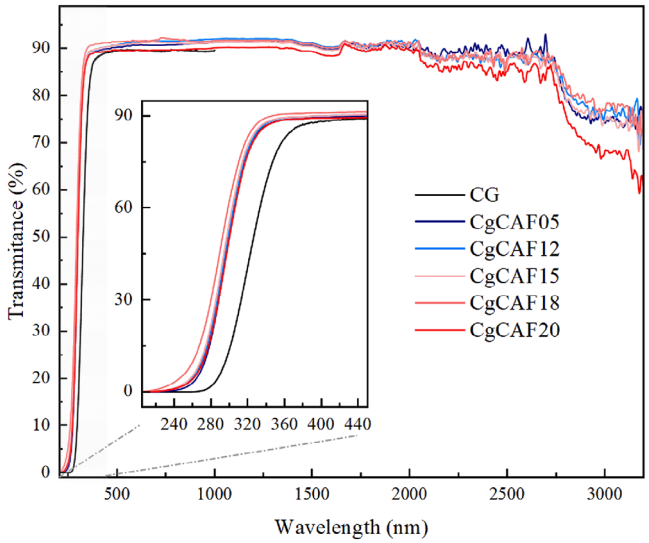

FIGURE 7 UV–VIS spectra.

4 | CONCLUSIONS

In this work, we have demonstrated the utilization of end-of-life cover glass from commercial solar panels to produce oxyfluoride glasses by incorporating CaF_2. XRF analyses have proven that the final samples are free of contaminants, such as iron, that could introduce color to the material, reducing its value and limiting its potential applications. This confirms that, due to the high purity and transparency of the soda-lime cover glass, we could use it to make up to 80% of the total weight of CgCAF glasses. In contrast, conventional flat glass production allows only a small proportion of the material to be recycled. Furthermore, the melting temperature of the samples was about 1200°C, significantly lower than the melting temperature of soda-lime glass, which favors a reduced energy consumption and carbon emissions to produce CgCAF samples. Thermal analysis showed a 50–90°C reduction in T_g temperature relative to the soda-lime, the presence of at least two crystallization processes and a pretty good stability of the glass phase, demonstrated by $(T_x–T_g)$ values in the range 100–180°C. XRPD confirmed the glassy nature of the samples and indicated a depolymerization process as the CaF_2 concentration increases, which is corroborated by mass density and Raman data. In situ XRPD measurements in the CgCAF12 sample demonstrated the formation of combeite, diopside, and Ca_3SiO_5 triclinic phases, besides some unidentified peaks that require further studies. Finally, the UV–Vis–NIR transmittance demonstrated the good optical quality of all samples and the improved UV transmittance window compared to the original CG employed in this work. The ensemble of results shows that this family of materials can be explored as glass or be crystallized to produce glass-ceramics that may be tailored for different applications. Further studies should focus on understanding the crystallization process of these materials and incorporating optically active ions. If scaled for practical applications, these oxyfluoride glasses could provide a viable route for the reintegration of end-of-life cover glass into the industrial value chain. Such an approach would not only enhance the economic value of this waste material but also promote circularity and sustainability within the glass and photovoltaic industries.

ACKNOWLEDGMENTS

The authors thank CNPq (grants 409475/2021-1, 402473/2023-0, and 304060/2023-2) for the financial support.

ORCID

Rafaela Valcarenghi https://orcid.org/0009-0007-4846-7493
Anna Paulla Simon https://orcid.org/0000-0002-4499-3281
Mathieu Allix https://orcid.org/0000-0001-9317-1316
Marcelo Sandrini https://orcid.org/0000-0001-9084-8117
Marcos Paulo Belançon https://orcid.org/0000-0001-5018-2613

REFERENCES

1. Rio DDFD, Sovacool BK, Foley AM, Griffiths S, Bazilian M, Kim J, Rooney D. Decarbonizing the glass industry: a critical and systematic review of developments. sociotechnical systems and policy options. Renewable Sustainable Energy Rev. 2022;155:111885. https://doi.org/10.1016/j.rser.2021.111885
2. Zier M, Stenzel P, Kotzur L, Stolten D. A review of decarbonization options for the glass industry. Energy Conversion Manag: X. 2021;10:100083. https://doi.org/10.1016/j.ecmx.2021.100083
3. Butler JH, Hooper PD. Glass Waste. 2nd ed. Amsterdam, the Netherlands: Elsevier; 2019, pp. 307–22. https://doi.org/10.1016/B978-0-12-815060-3.00015-3 https://linkinghub.elsevier.com/retrieve/pii/B9780128150603000153
4. Caudle B, Taniguchi S, Nguyen TT, Kataoka S. Integrating carbon capture and utilization into the glass industry: economic analysis of emissions reduction through CO_2 mineralization. J Cleaner Prod. 2023;416:137846. https://doi.org/10.1016/j.jclepro.2023.137846 https://linkinghub.elsevier.com/retrieve/pii/S0959652623020048
5. Westbroek CD, Bitting J, Craglia M, Azevedo JMC, Cullen JM. Global material flow analysis of glass: from raw materials to end of life. J Ind Ecol. 2021;25333–343. https://doi.org/10.1111/jiec.13112
6. Bristogianni T, Oikonomopoulou F. Glass up-casting: a review on the current challenges in glass recycling and a novel approach for recycling "as-is" glass waste into volumetric glass components. Glass Struct Eng. 2023;8255–302. https://doi.org/10.1007/s40940-022-00206-9
7. Belançon MP, Sandrini M, Zanuto VS, Muniz RF. Glassy materials for silicon-based solar panels: present and future.

J Non Cryst Solids. 2023;619:122548. https://doi.org/10.1016/j.jnoncrysol.2023.122548 https://linkinghub.elsevier.com/retrieve/pii/S0022309323004143

8. Li X, Gu Q, Wang Q, Luo J, Liu D, Chang Y. Renewable energy in the mining industry: Status, opportunities and challenges. Energy Strategy Rev. 2024;56:101597. https://doi.org/10.1016/j.esr.2024.101597 https://www.sciencedirect.com/science/article/pii/S2211467X24003067
9. Gaustad G, Krystofik M, Bustamante M, Badami K. Circular economy strategies for mitigating critical material supply issues. Resour Conserv Recycl. 2018;135:24-33. https://doi.org/10.1016/j.resconrec.2017.08.002
10. Sica D, Malandrino O, Supino S, Testa M, Lucchetti MC. Management of end-of-life photovoltaic panels as a step towards a circular economy. Renewable Sustainable Energy Rev. 2018;82:2934-45. https://doi.org/10.1016/j.rser.2017.10.039
11. Zink T, Geyer R. Material recycling and the myth of landfill diversion. J Ind Ecol. 2019;23:541-48. https://doi.org/10.1111/jiec.12808
12. Muniz RF, Greatti BS, Sandrini M, Belançon MP, Valcarenghi R, Bini RD, Zanuto VS. Glass Application in Solar Energy Technology. London: IntechOpen; 2025. https://doi.org/10.5772/intechopen.1010177 https://www.intechopen.com/online-first/1218426
13. Muniz RF, Soares VO, Montagnini GH, Medina AN, Baesso ML. Thermal, optical and structural properties of relatively depolymerized sodium calcium silicate glass and glass-ceramic containing CaF_2. Ceram Int. 2021;47:24966–72. https://doi.org/10.1016/j.ceramint.2021.05.224
14. Muniz RF, Steimacher A, Pedrochi F, Zanuto VS, Azevedo LM, Rohling JH, Baesso ML, Medina AN. Eu^{2+}-Nd^{3+} co-doped glasses for solar spectrum modification via NUV/visible to NIR downconversion. J Alloys Compd. 2021;888:161484. https://doi.org/10.1016/j.jallcom.2021.161484
15. Zheng J, Xing X, Liu W, Pang Z, Hu R, Xue Q, Wang J, Zuo H. An integrate study of the effects of CaF_2 on the viscous behavior and structure of CaO-SiO_2-MgO-Al_2O_3 – CaF_2 blast-furnace slag. J Non Cryst Solids. 2025;648:123310. https://doi.org/10.1016/j.jnoncrysol.2024.123310
16. Riaz M, Zia R, Mirza A, Hussain T, Bashir F, Anjum S. Synthesis, characterization of CaF_2 doped silicate glass-ceramics. Mater Sci Eng, C. 2017;75:872–76. https://doi.org/10.1016/j.msec.2017.02.141 https://linkinghub.elsevier.com/retrieve/pii/S0928493116319798
17. Xu J, Chen P. Effect of crystallization behavior and phase evolution on glass-ceramics derived from alumina silicate solid waste with addition high content CaF_2. Chem Eng J. 2025;506:159998. https://doi.org/10.1016/j.cej.2025.159998
18. Laonamsai J, Tasi P, Wiwatrojanagul P, Sriondee M, Suriwong T, Julphunthong P. Synergistic effects of CuO and CaF_2 additives in facilitating low-temperature tricalcium silicate formation and stabilization. Results Eng. 2025;26:104620. https://doi.org/10.1016/j.rineng.2025.104620
19. Pawlik N, Szpikowska-Sroka B, Goryczka T, Pisarska J, Pisarski WA. Structural and photoluminescence investigations of Tb^{3+}/Eu^{3+} co-doped silicate sol-gel glass-ceramics containing CaF_2 nanocrystals. Materials. 2021;14:754. https://doi.org/10.3390/ma14040754
20. Belançon MP, Sandrini M, Tonholi F, Herculano LS, Dias GS. Towards long term sustainability of C-Si solar panels: the environmental benefits of glass sheet recovery. Renewable Energy Focus. 2022;42:206–10. https://doi.org/10.1016/j.ref.2022.06.009 https://linkinghub.elsevier.com/retrieve/pii/S1755008422000515
21. de Almeida RPF, Bocker C, Rüssel C. Size of CaF_2 crystals precipitated from glasses in the Na_2O/K_2O/CaO/CaF_2/Al_2O3/SiO_2 system and percolation theory. Chem Mater. 2008;20:5916–21. https://doi.org/10.1021/cm801426u
22. Rüssel C. Nanocrystallization of CaF_2 from Na_2O/K_2O/CaO/CaF_2/Al_2O3/SiO_2 glasses. Chem Mater. 2005;17:5843–47. https://doi.org/10.1021/cm051430x
23. Iwamoto N, Makino Y. A structural investigation of calcium fluorosilicate glasses. J Non Cryst Solids. 1981;46(1):81–94. https://doi.org/10.1016/0022-3093(81)90076-4
24. Caland JP, Baptista J, Peiter GC, de Aguiar KM, Coelho-Júnior H, Sinnecker JP, Felix JF, Schneider R. Nanostructured glass-ceramic materials from glass waste with antimicrobial activity. Molecules. 2024;29(13):3212. https://doi.org/10.3390/molecules29133212
25. Vidal L, Joussein E, Colas M, Cornette J, Sanz J, Sobrados I, Gelet JL, Absi J, Rossignol S. Controlling the reactivity of silicate solutions: a FTIR, Raman and NMR study. Colloids Surf A. 2016;503:101–9. https://doi.org/10.1016/j.colsurfa.2016.05.039
26. Gao J, Wen G, Huang T, Bai B, Tang P, Liu Q. Effect of slag-steel reaction on the structure and viscosity of CaO-SiO_2-based mold flux during high-Al steel casting. J Non Cryst Solids. 2016;452:119–24. https://doi.org/10.1016/j.jnoncrysol.2016.08.036 https://linkinghub.elsevier.com/retrieve/pii/S0022309316303611
27. Tian H, Wang Z, Zhao T, Wang C. A Raman and multinuclear 29Si, 27Al, and 19F NMR study on the structural roles of CaF_2 in SiO_2–CaO–Al_2O3-based welding fluxes. Metall Mater Trans B. 2022;53:232–41. https://doi.org/10.1007/s11663-021-02359-4
28. Yadav AK, Singh P. A review of the structures of oxide glasses by Raman spectroscopy, RSC Adv. 2015;5:67583–609. https://doi.org/10.1039/c5ra13043c
29. Tsunawaki Y, Iwamoto N, Hattori T, Mitsuishi A. Analysis of CaO_2 SiO_2 and CaO_2 SiO_2CaF_2 glasses by Raman spectroscopy. J Non Cryst Solids. 1981;44(2–3):369–78. https://doi.org/10.1016/0022-3093(81)90039-9
30. Luth RW. Raman spectroscopic study of the solubility mechanisms of F in glasses in the system CaO-CaF_2 – SiO_2. Am Mineral. 1988;73(3–4):297–305.
31. Muniz R, Baesso M, Sato F, Bento A, Rohling J, Medina A. High pressure effect on the short-and intermediate-range structure of depolymerized soda-lime silicate glass: insights from micro-Raman spectroscopy. Vib Spectrosc. 2020;110:103113. https://doi.org/10.1016/j.vibspec.2020.103113
32. Dumas P, Corset J, Levy Y, Neuman V. Raman spectral characterization of pure and fluorine-doped vitreous silica material. J Raman Spectrosc. 1982;13(2):134–38. https://doi.org/10.1002/jrs.1250130207
33. Wang M, CHeng J, Li M, He F. Raman spectra of soda–lime–silicate glass doped with rare earth. Physica B. 2011;406(20):3865–69. https://doi.org/10.1016/j.physb.2011.07.014
34. Novatski A, Steimacher A, Medina AN, Bento AC, Baesso ML, Andrade LHC, Lima SM, Guyot Y, Boulon G. Relations

among nonbridging oxygen, optical properties, optical basicity, and color center formation in CaO–MgO aluminosilicate glasses. J Appl Phys. 2008;104(9):094910. https://doi.org/10.1063/1.3010306 https://pubs.aip.org/jap/article/104/9/094910/389590/Relations-among-nonbridging-oxygen-optical

35. O'Shaughnessy C, Henderson GS, Nesbitt HW, Bancroft GM, Neuville DR. The influence of modifier cations on the Raman stretching modes of Qn species in alkali silicate glasses. J Am Ceram Soc. 2020;103:3991-4001. https://doi.org/10.1111/jace.17081
36. Boizot B, Agnello S, Reynard B, Boscaino R, Petite G. Raman spectroscopy study of β-irradiated silica glass. J Non Cryst Solids. 2003;325(1–3):22–8. https://doi.org/10.1016/S0022-3093(03)00334-X

How to cite this article: Valcarenghi R, Greatti BS, Muniz RF, Zanuto VS, Simon AP, Schneider R, et al. Oxyfluoride glasses obtained through incorporation of CaF_2 into photovoltaic cover glass melts. J Am Ceram Soc. 2025;e70252. https://doi.org/10.1111/jace.70252